

Nonlinear model reduction using multiple expansion bases

By M. Fosas de Pando[†], P.J. Schmid[‡] AND S.K. Lele

Nonlinear model reduction is a critical component in the design process of control strategies for complex flows in the nonlinear regime. A Galerkin projection based on POD-modes is developed in this study that takes advantage of multiple bases for particular components of the governing equations. These bases are then linked by the Discrete Empirical Interpolation Method (DEIM) to ultimately arrive at a reduced-order, nonlinear dynamic system that does no longer contain full-degree-of-freedom operations. Two test cases are included: the compressible flow in the wake of a NACA-0012 airfoil and a compressible impinging two-dimensional jet. Promising results have been obtained for both cases.

1. Motivation and background

Model reduction is an important component in many applications related to fluid system as it is concerned with the accurate representation of fluid dynamical behavior with far fewer degrees of freedom than are present in full nonlinear simulations (Antoulas 2004; Quarteroni & Rozza 2014). This methodology is particularly important in flow control applications where predictions of the future evolution of the fluid system (often under control input) are used to design a control strategy that achieves a prescribed set of cost objectives. The evaluation of these predictions has to be performed in real time, and a control strategy has to be determined in a short time frame. For this reason, approximate but sufficiently accurate predictions of the flow have to be made with reduced-order models (ROMs) representing the full flow physics (Ito & Ravindran 1998; Ravindran 2002; Samimy *et al.* 2007; Barbagallo *et al.* 2009; Lassila *et al.* 2014).

In the case of fluid systems that are aptly described by a globally stable, linear set of equations (also referred to as an amplifier flow), well known techniques exist that preserve the essential dynamics between the control input and the measurement output while reducing a high-dimensional system to a low-dimensional one. For unstable configurations, on the other hand, where nonlinearities lead to limit-cycle behavior with saturated oscillations, the procedural steps for an effective model reduction are less obvious and less explored. Even though techniques extended from a linear framework have been applied to nonlinear large-scale systems, there remains a computational bottleneck when evaluating the nonlinear terms of the equations. This evaluation often scales with the number of degrees-of-freedom of the full system, excises the gains from the linear terms, and compromises computational efficiency of the final reduced-order model. A recent technique (Chaturantabut & Sorensen 2010, 2011) suggests the Galerkin expansion of the nonlinear terms in a basis that is distinct from the basis for the full system. In addition, the nonlinear terms in this second basis are evaluated on judiciously selected interpolation

[†] Department of Mechanical Engineering and Industrial Design, Universidad de Cádiz, Spain

[‡] Department of Mathematics, Imperial College London, United Kingdom

points, thus avoiding the above-mentioned bottleneck. The choice of these interpolation points is made using a greedy algorithm that optimizes the error in the representation of the nonlinear terms. This technique, known as the proper-orthogonal-decomposition discrete-empirical-interpolation method (POD-DEIM), has been applied and illustrated on systems of ordinary and partial differential equations and has shown great potential in accurately representing the full system dynamics with remarkably few degrees of freedom.

An application of this technique to large-scale, complex fluid systems has not yet been attempted. In addition, the nature of nonlinearities encountered in fluid systems required supplementary steps and the introduction of virtual, auxiliary variables during the reduction process. Furthermore, for an efficient implementation, the model reduction algorithm is to be embedded in an automated framework developed for the computation of linearized and adjoint dynamics (Fosas de Pando *et al.* 2012); in fact, it will be merged with this technology to provide complete, fast, and robust access to flow information.

2. Mathematical background

The Discrete Empirical Interpolation Method (DEIM) was recently introduced by Chaturantabut & Sorensen (2010). It relies on the use of proper orthogonal decomposition (POD) modes for the representation of the full-system dynamics as well as supplementary bases for the specific representation of local nonlinearities. The link between these two bases is established by the evaluation of the nonlinear expansion at selected interpolation points are chosen by a greedy algorithm to reduce the residual error.

In Chaturantabut & Sorensen (2010), the authors introduce the POD-DEIM technique to generate reduced-order models for nonlinear partial differential equations directly from a system of nonlinear ordinary differential equations that typically arise from the spatial discretization. The starting point is a coupled system of nonlinear ordinary differential equations of the form

$$\frac{d\mathbf{y}(t)}{dt} = \mathbf{A}\mathbf{y}(t) + \mathbf{F}(\mathbf{y}(t)), \quad (2.1)$$

where $\mathbf{y}(t)$ is the state vector containing all pertinent flow field information in form of a vector with n entries, \mathbf{A} stands for a $n \times n$ matrix capturing the linear part of the dynamics, and $\mathbf{F}(\mathbf{y})$ denotes a component-wise nonlinear function of $\mathbf{y}(t)$.

Integrating in time, a first POD basis \mathbf{V} is generated from the leading k modes of the POD decomposition (singular value decomposition) of the temporal evolution of $\mathbf{y}(t)$. We assume $k \ll n$. The state vector $\mathbf{y}(t)$ is then approximated in this basis by $\mathbf{V}\tilde{\mathbf{y}}(t)$ and the governing equations are projected onto the basis \mathbf{V} (note that by design $\mathbf{V}^H\mathbf{V} = \mathbf{I}$). Hence,

$$\frac{d\tilde{\mathbf{y}}(t)}{dt} = \mathbf{V}^H\mathbf{A}\mathbf{V}\tilde{\mathbf{y}}(t) + \mathbf{V}^H\mathbf{F}(\mathbf{V}\tilde{\mathbf{y}}(t)). \quad (2.2)$$

Even though the cost of evaluating the linear terms on the right-hand side has been reduced to $\mathcal{O}(k^2)$ operations, the cost of evaluating the nonlinear terms typically requires $\mathcal{O}(n)$ operations. To further reduce the operation count, a second basis, \mathbf{U} , is generated from the leading l modes from the POD decomposition of the sequence of nonlinear snapshots given by $\mathbf{F}(\mathbf{y}(t))$. In Chaturantabut & Sorensen (2010), the authors attempt to approximate $\mathbf{F}(\mathbf{y}(t))$ by the most suitable element in the space spanned by \mathbf{U} , which is equivalent to determining $\tilde{\mathbf{c}}(t)$ from $\mathbf{F}(\mathbf{y}(t)) \approx \mathbf{U}\tilde{\mathbf{c}}(t)$. For this purpose, they introduce so-called interpolation points, where the above relationship must be satisfied exactly. We shall later summarize the procedure that allows us to choose the interpolation points.

For now, let us assume that \mathbf{P} is a $n \times l$ matrix whose columns are unit vectors in \mathbb{R}^n that, when multiplied to a vector, select a given element of this vector. Matrix \mathbf{P} is thus referred to as a row-selector matrix, and the selected points are the above-mentioned interpolation points. The DEIM approximation then reads

$$\tilde{\mathbf{c}}(t) = (\mathbf{P}^T \mathbf{U})^{-1} \mathbf{P}^T \mathbf{F}(\mathbf{V} \tilde{\mathbf{y}}(t)). \quad (2.3)$$

It is worth noting that, because $\mathbf{F}(\cdot)$ is a component-wise function, it is required only to evaluate the nonlinear function at the interpolation points. Hence, $\mathbf{P}^T \mathbf{F}(\mathbf{V} \tilde{\mathbf{y}}(t)) = \mathbf{F}(\mathbf{P}^T \mathbf{V} \tilde{\mathbf{y}}(t))$. At last, the nonlinear reduced-order model reads

$$\frac{d\tilde{\mathbf{y}}(t)}{dt} = \mathbf{V}^H \mathbf{A} \mathbf{V} \tilde{\mathbf{y}}(t) + (\mathbf{V}^H \mathbf{U}) (\mathbf{P}^T \mathbf{U})^{-1} \mathbf{F}(\mathbf{P}^T \mathbf{V} \tilde{\mathbf{y}}(t)). \quad (2.4)$$

At this point, it only remains to provide an algorithm to select the interpolation points \mathbf{k} and the row selector matrix \mathbf{P} . To this end, we use the procedure given in Chaturantabut & Sorensen (2010) that, given a rectangular matrix of basis vectors, employs a greedy algorithm to successively choose the maximum of the absolute value of the current residual approximation to the nonlinear basis. The interested reader is referred to Chaturantabut & Sorensen (2010) for additional details.

It is important to stress that the assumption of a component-wise nonlinearity \mathbf{F} has been instrumental in evaluating the nonlinearities only at the DEIM-interpolation points -a crucial step in arriving at a nonlinear, reduced-order model-. For applications to the compressible Navier-Stokes equations this assumption no longer holds: the type of nonlinear terms contained in the governing equations are far more complicated, and, as a consequence, the procedure outlined above does not directly apply. In Chaturantabut & Sorensen (2010) the authors nevertheless provide an extension to the DEIM technique that permits the consideration of general non-component-wise nonlinearities. Typically, during the discretization of nonlinear terms, differential operators in continuous form are replaced by their discrete counterparts. These approximations introduce a nonlocal spatial dependence and yield nonlinear terms of the form $\mathbf{f}_i(\mathbf{y}_j)$ where the \mathbf{y}_j denotes each state variable, i.e., \mathbf{y}_j , the components of vector \mathbf{y} that are required to evaluate the nonlinear terms. Following the same procedure, the authors then introduce sparse matrices to take into account the dependence on the different grid points. However, such an approach relies on the sparsity of the spatial discretization. In flow solvers that feature high-order schemes, these matrices are in general dense, and the above approach becomes impractical because the matrices typically exceed the available storage capacity. Similar drawbacks are also encountered in the derivation of linearized operators and the implementation of the adjoint operator: starting from a compressible flow solver, these matrices are in general dense and largely surpass available storage resources.

To demonstrate the novel approach in extending the existing model reduction procedure for nonlocal nonlinearities, we focus first on the treatment of typical advection terms encountered in the Navier-Stokes equations $\mathbf{u} \cdot \nabla \mathbf{u}$, given for the two-dimensional case as

$$f_1(u, v) = u \partial_x u + v \partial_y u, \quad (2.5a)$$

$$f_2(u, v) = u \partial_x v + v \partial_y v. \quad (2.5b)$$

Once discretized, these equations can be rewritten as

$$\mathbf{F}(\mathbf{v}) = [\mathbf{D}_x \mathbf{v} \quad \mathbf{D}_y \mathbf{v}] \mathbf{v}, \quad (2.6)$$

where \mathbf{D} represents a suitable finite-difference differentiation scheme. It should be noted

that, prior to discretization, the values of velocity and velocity gradients are pointwise. However, once differentiation schemes have been introduced, this dependence becomes global. It must be emphasized that this global dependence is caused by the differentiation matrix \mathbf{D} . In most high-order finite-difference approximations, the corresponding differentiation matrix \mathbf{D} either has a large bandwidth, or is dense. The question that has to be addressed is how to perform a POD-DEIM reduction of Eq. (2.6). We start with

$$\mathbf{f}(\mathbf{v}) = [\mathbf{D}_x \mathbf{v} | \mathbf{D}_y \mathbf{v}] \mathbf{v}, \quad (2.7a)$$

$$\mathbf{f}(\mathbf{V}\tilde{\mathbf{v}}) \approx \mathbf{U}(\mathbf{P}^T \mathbf{U})^{-1} \mathbf{P}^T \mathbf{f}(\mathbf{V}\tilde{\mathbf{v}}), \quad (2.7b)$$

but because \mathbf{f} is not pointwise, we are not justified in applying the row-selector matrix \mathbf{P}^T to the argument of the function \mathbf{f} . Nevertheless, \mathbf{f} can be restated in a manner that allows us to identify pointwise nonlinear terms.

We introduce auxiliary variables \mathbf{r} and \mathbf{s} such that $\mathbf{r} = \mathbf{D}_x \mathbf{v}$, $\mathbf{s} = \mathbf{D}_y \mathbf{v}$ and redefine the function $\mathbf{f}(\mathbf{v}, \mathbf{r}, \mathbf{s}) = [\mathbf{r} | \mathbf{s}] \mathbf{v}$ in terms of these new variables. Algorithmically, we compute the nonlinear terms in the following two steps

$$\mathbf{r}, \mathbf{s} \leftarrow \mathbf{D}_x \mathbf{u}, \mathbf{D}_y \mathbf{u}, \quad (2.8a)$$

$$\mathbf{F}(\mathbf{v}, \mathbf{r}, \mathbf{s}) = [\mathbf{r} \quad \mathbf{s}] \mathbf{v}. \quad (2.8b)$$

Then, in the reduced-order system we obtain terms of the form

$$\mathbf{f}(\mathbf{V}\tilde{\mathbf{v}}, \mathbf{D}_x \mathbf{V}\tilde{\mathbf{v}}, \mathbf{D}_y \mathbf{V}\tilde{\mathbf{v}}) \approx \mathbf{U}(\mathbf{P}^T \mathbf{U})^{-1} \mathbf{f}(\mathbf{P}^T \mathbf{V}\tilde{\mathbf{v}}, \mathbf{P}^T \mathbf{D}_x \mathbf{V}\tilde{\mathbf{v}}, \mathbf{P}^T \mathbf{D}_y \mathbf{V}\tilde{\mathbf{v}})$$

or, using a more compact notation,

$$\mathbf{f}(\mathbf{V}_k \tilde{\mathbf{v}}) \approx \mathbf{U}(\mathbf{P}^T \mathbf{U})^{-1} \mathbf{f}(\mathbf{P}^T \mathbf{V}_k \tilde{\mathbf{v}}) \quad \text{with} \quad \mathbf{V}_k = \mathbf{D}_k \mathbf{V}, \quad (2.9)$$

where $(\mathbf{P}^T \mathbf{V}_k)$ represents the spatial derivatives of the basis \mathbf{V} at the interpolation points. In the remaining of the paper, the basis \mathbf{U} introduced above will be denoted \mathbf{U}_0 .

In addition to the extension sketched before, for general types of nonlinear terms, multiple nonlinear bases need to be introduced to fully reduce the original system. To further illustrate this point, we consider our implementation of the compressible Navier–Stokes equations written in pressure, entropy and velocity formulation. Although the heat dissipation term $\nabla \cdot (k \nabla T(p, s))$ is linear in the temperature variable T , this term is nonlinear in pressure and entropy variables, which renders the heat flux in our implementation a nonlinear function. To reduce in order, we suggest the introduction of additional intermediate variables, such as the heat flux $\mathbf{q} = -k \nabla T(p, s)$, and an additional nonlinear basis, i.e., \mathbf{U}_1 , to provide a low-rank approximation of nonlinearities in the heat dissipation terms. This approach provides us with an efficient technique to construct reduced-order models of governing equations with a broader family of nonlinear terms such as turbulence models, temperature-dependent viscosities, and reactive terms, etc.

In the above procedure, we have stated governing equations consisting of a linear and a nonlinear part. This partition between linear and nonlinear terms, however, is not unique. In typical applications of interest, a reference state is given — typically a steady state or a mean flow — and we focus our attention on the evolution of a disturbance about this state. Following a common notation, we decompose our flow field into a reference state $\bar{\mathbf{v}}$ and disturbances \mathbf{v}' . We then add and subtract the first two terms of a Taylor series expansion around the reference field $\bar{\mathbf{v}}$, i.e., $\pm(\mathbf{f}(\bar{\mathbf{v}}_k) + \mathbf{A}\mathbf{v}')$, where $\mathbf{A}\mathbf{v}' = \left. \frac{\partial \mathbf{f}}{\partial \mathbf{v}_k} \right|_{\bar{\mathbf{v}}_k} \mathbf{v}'$. We

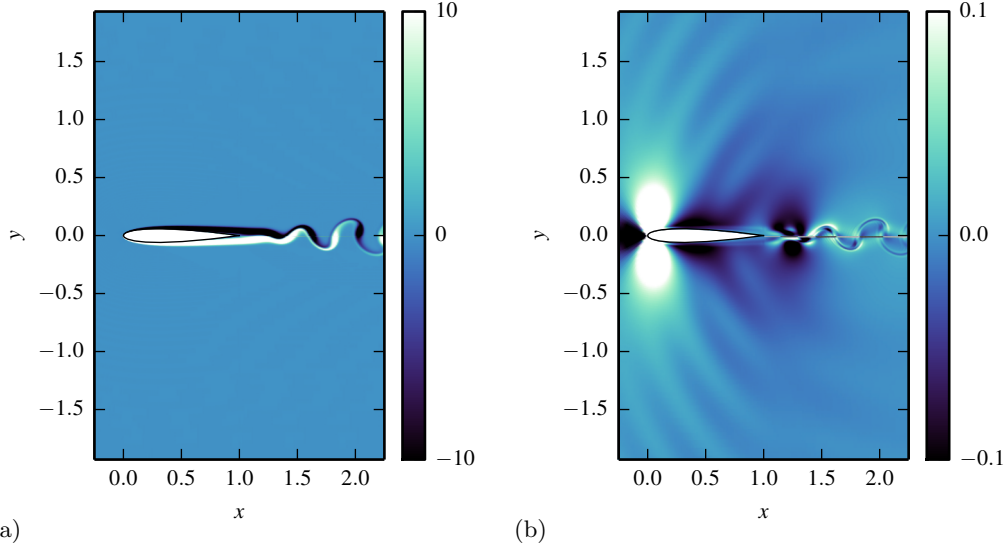


FIGURE 1. Instantaneous flow field depicted by (a) vorticity field showing periodic vortex shedding into the wake and (b) dilatation field showing significant upstream sound directivity. See text for parameter values.

thus have

$$\underbrace{\mathbf{f}(\bar{\mathbf{v}}_k) + \mathbf{A}\mathbf{v}'}_{\text{const+linear}} + \underbrace{[\mathbf{f}(\bar{\mathbf{v}}_k + \mathbf{v}'_k) - (\mathbf{f}(\bar{\mathbf{v}}_k) + \mathbf{A}\mathbf{v}')] }_{\text{nonlinear}}. \quad (2.10)$$

3. Application to flow around an airfoil

We now apply the nonlinear model-reduction technique based on POD-DEIM to the two-dimensional compressible flow around a NACA-0012 airfoil without incidence. The chord-based Reynolds number is $\text{Re} = 10000$, the Mach number is $M = 0.6$, the heat capacity ratio is $\gamma = 1.4$, and the Prandtl number is $\text{Pr} = 0.71$. In order to obtain a reduced-order model, it is first necessary to generate the dataset from which the different POD bases will be obtained. To this end, we have first simulated this flow using an in-house compressible Navier–Stokes numerical solver. The reference values for the nondimensionalization are those of the unperturbed flow (except for the entropy, where the ideal gas constant r has been taken as the reference value), the reference length-scale is the aerofoil chord, and the temporal scale is the residence time over one unit length. The resulting dynamical system consist of $m = 10^6$ degrees of freedom, and it has been integrated in time from a suitable initial condition until transients have vanished and a periodically steady-state has been established ($t \approx 100$). The subsequent flow evolution has been stored every $\Delta = 0.01$ from $t_0 = 100$ to $t_f = 105$ yielding a total of $n = 500$ snapshots. Figure 1 illustrates the features of the periodically steady state: the vorticity component ω_z displays vortex shedding downstream the aerofoil along the wake, and the dilatation field $d = u_x + v_y$ shows acoustic radiation from the trailing edge with preferred upstream directionality.

To establish the different set of bases, i.e., \mathbf{V} , \mathbf{U}_0 , and \mathbf{U}_1 , the required snapshot sequences have to be generated from the flow field snapshots $\{\mathbf{v}_i\}_{i=1}^n$. The basis \mathbf{V} has been

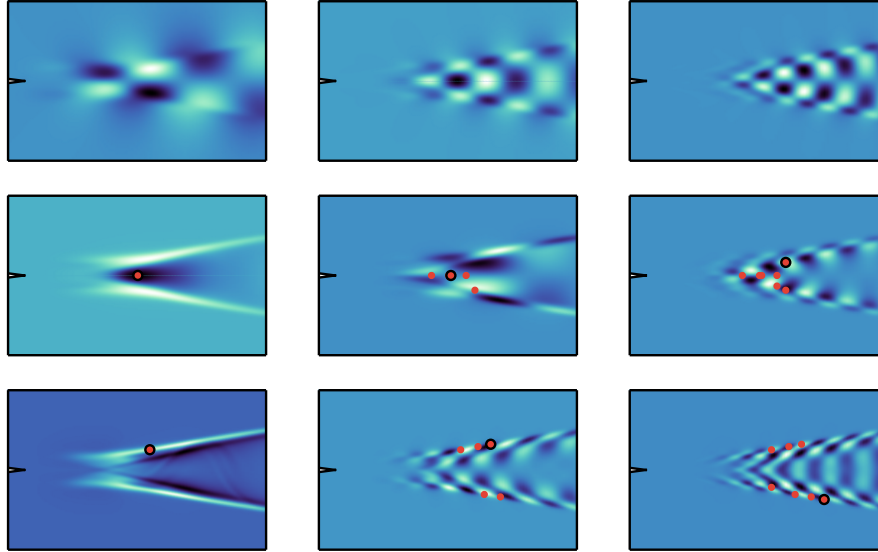


FIGURE 2. (top row) Selected modes from the POD basis \mathbf{V} of the snapshot series, visualized by the streamwise velocity component. (middle row) POD basis \mathbf{U}_0 of the nonlinear snapshots showing the streamwise velocity component. (bottom row) POD basis \mathbf{U}_1 of the nonlinear snapshots showing the streamwise component of the heat flux. The interpolation points selected by the DEIM algorithm are also represented.

generated by computing the proper orthogonal decomposition of the snapshots $\{\mathbf{v}'_i\}_{i=1}^n$, where \mathbf{v}'_i is the difference between the instantaneous flow field \mathbf{v}_i and the time-averaged flow $\bar{\mathbf{v}}$.

In Figure 2 the leading vectors of the basis \mathbf{V} are displayed (top row) in terms of the perturbation streamwise velocity component u' . All the modes display spatial support in the wake, with a characteristic wavelength and symmetry patterns: modes $2i$ and $2i + 1$ with i odd have an antisymmetric streamwise and pressure component, and symmetric vertical velocity component with respect to x -axis. The converse is true for modes $2i$ and $2i + 1$ with k even, and higher values of i are associated with higher spatial wavenumbers. Modes (1, 2) are the only ones that display acoustic radiation in the far field (not shown). In Figure 2(middle row) the leading vectors of the basis \mathbf{U} are represented in terms of the streamwise velocity component together with the DEIM points. The vector basis for the nonlinear terms \mathbf{U} has been obtained from the Proper Orthogonal Decomposition of the snapshots $\{\mathbf{f}'(\mathbf{v}_i)\}_{i=1}^n$ of the nonlinear terms.

Following the above procedure, we were able to reduce the nonlinear simulations to a nonlinear dynamical system with 16 degrees of freedom, while maintaining the maximum relative residual ϵ_{rel} below 10^{-2} . Results from the simulations and the reduced-order model are shown in Figure 3 as a function of the order of the ROM (left) as well as a spatial distribution of the relative residual (right). A further validation of the reduced-order model consists of a frequential analysis of the time signals extracted at various points of the computational domain. These time signals have been generated either by the full nonlinear simulation (with $m = 10^6$ degrees of freedom) or by the reduced-order model (with only 16 degrees of freedom). Three cases are shown in Figure 4. The first signal has been extracted in the far field above the trailing edge, intended to capture the acoustic

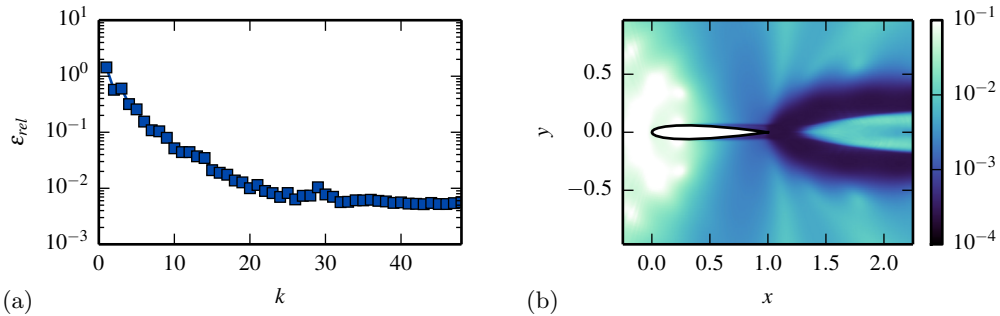


FIGURE 3. (a) Local relative error of the reduced order model compared to the numerical simulation, as a function of the dimension of the reduced-order model (ROM). (b) Spatial distribution of the relative residual. In both cases, the mean value has been subtracted.

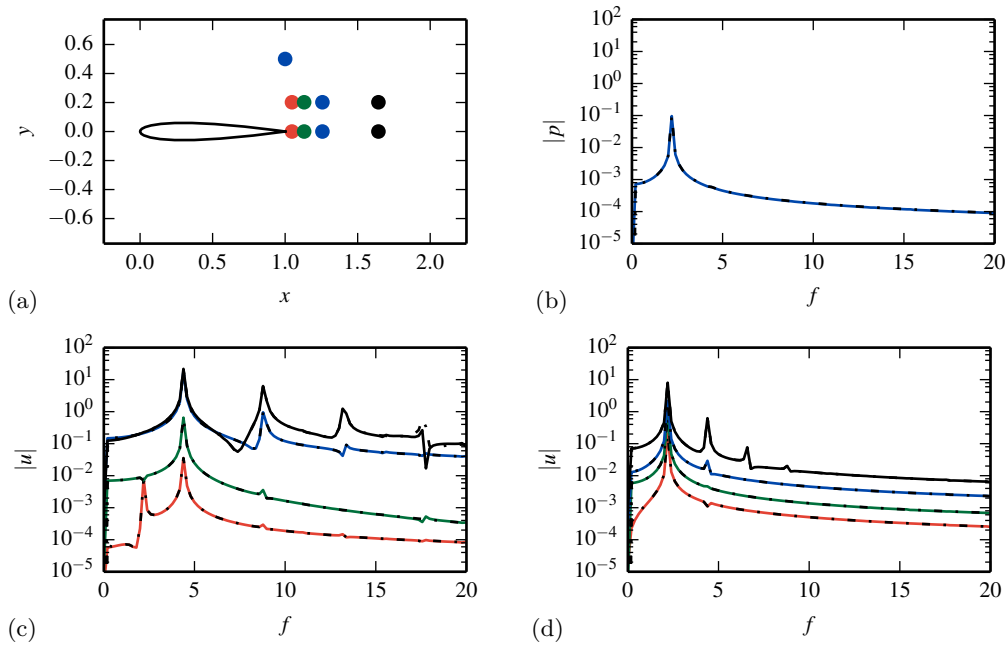


FIGURE 4. Comparison between the frequency spectrum of time-signals from the original numerical simulation and the reduced order models at selected extraction points. (a) Locations of measurement probes, (b) pressure spectrum at far-field point above trailing edge, (c) stream-wise-velocity component frequency content for the probes along the wake, (d) streamwise-velocity component frequency content at a moderate distance from the wake. The results from the full system are indicated by the dashed line.

footprint of the wake dynamics; the second set of signals has been placed in the wake to validate the reproduction of the wake dynamics; the third set of signals, at a moderate distance about the center of the wake, extracts information from the near field of the wake. All time signals have been Fourier transformed, and the results from the reduced-order model show excellent agreement with the corresponding power spectral densities of the full direct numerical simulations at the measurement locations.

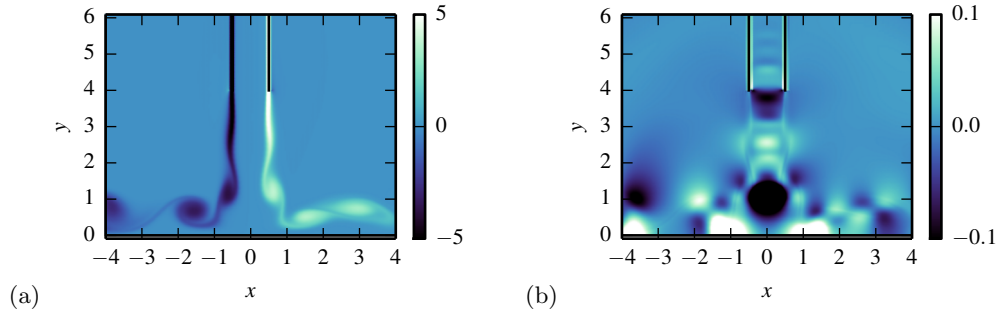


FIGURE 5. Instantaneous flow field of a compressible impinging jet, visualized by (a) vorticity contours, and (b) contours of the dilatation field.

4. Application to a high-speed subsonic impinging jet

A more challenging configuration for demonstrating the nonlinear model-reduction technique consists of a two-dimensional compressible jet with normal impingement on a wall. The jet width has been taken as the spatial length-scale, and the distance between the jet outlet plane and the wall is $h = 4$. The Reynolds number based on the jet width is $Re = 1875$, the Mach number is $M = 0.8$, the heat capacity ratio is $\gamma = 1.4$, and the Prandtl number is $Pr = 0.71$. Sponge layers have been imposed in the far field to suppress spurious reflection of acoustic waves at the boundaries of the computational domain. Figure 5 displays two representative snapshots from the compressible simulations, showing the vorticity and dilatation field. As before, we extract POD-modes from simulations of the impinging jet. This is followed by preparing two bases for our nonlinear terms in the equation: the first capturing nonlinear convective effects, the second arising from the nonlinear nature of the heat flux in our pressure-entropy formulation. Representative fields for the three bases are shown in Figure 6; in addition, for the nonlinear bases we display the DEIM points where nonlinearities are evaluated.

As before, we validate the model reduction by generating time-signals from the reduced-order model and by comparing the spectral content to the equivalent values from the direct numerical simulation of the full system. To this end, we selected a group of probing points covering the jet exit, the stagnation region, the region where vortex pairing is observed, and the near field and the far field (see Figure 7(a) for a display of the probing points). The respective Fourier-transformed time-signals for pressure measurements, Figure 7(b), and streamwise-velocity measurements Figure 7(c), are shown in the same figure, with the results from DNS displayed with dashed lines and the corresponding curves from the reduced-order model in solid lines of the same color. Even though discrepancies are visible, the main features are very well captured, both in frequency and amplitude.

5. Conclusions

An efficient methodology has been developed for the nonlinear model reduction of large-scale compressible flow simulations. It is based on an earlier work (Chaturantabut & Sorensen 2010) and consists of POD-based Galerkin projections for multiple bases. These bases are tailored to specific features of the governing equation, in our case the nonlinear terms, to yield a more accurate and robust representation of the dynamic processes arising from these terms. The various bases are linked by the Discrete Empirical Interpolation Method (DEIM) that enforces the nonlinear terms at selected points, which in turn are

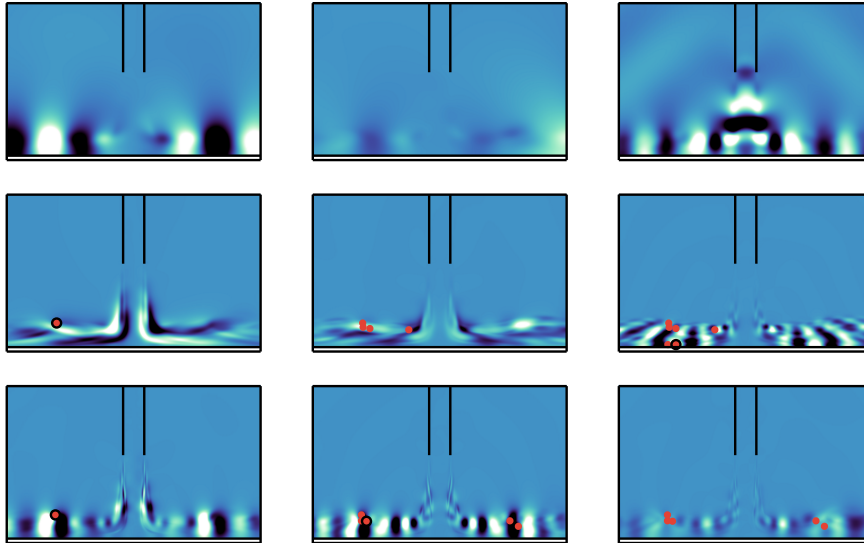


FIGURE 6. Selected modes from the full snapshot sequence (top row), from the nonlinear snapshot sequence capturing the nonlinear convective terms (middle row), from the nonlinear snapshot sequence representing the nonlinear heat flux (bottom row). For the nonlinear bases, the DEIM points are shown as well.

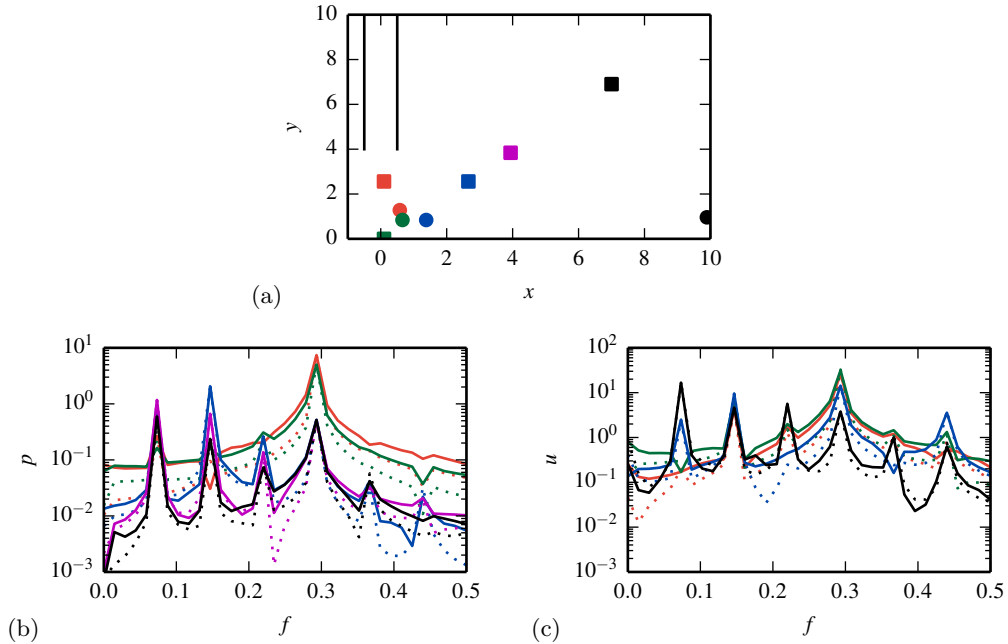


FIGURE 7. Comparison of the frequency spectrum of time-signals extracted from the original numerical simulation and the reduced order models at selected measurement points. (a) Sketch of jet configuration and measurement locations, (b) pressure spectrum (DNS-results in dashed lines, ROM-results in solid lines of corresponding color), (c) streamwise-velocity frequency content (DNS-results in dashed lines, ROM-results in solid lines of corresponding color).

chosen by a greedy algorithm to sequentially reduce the residual. The original model-reduction algorithm has been extended to account for nonlocal nonlinearities (encountered in simulations of compressible flow) by introducing auxiliary variables that are treated as independent and thus render nonlocal nonlinearities local. An efficient implementation, following our previous work (Fosas de Pando *et al.* 2012), has been achieved, that results in a flexible and adaptive framework for the model-reduction of complex flows. The compressible flow in the wake of a NACA0012 airfoil and the impingement of a subsonic jet on a flat wall have been chosen as validation cases for the nonlinear model-reduction technique. In both cases, reduced models with only a few degrees of freedom have been able to accurately capture the main features observed in the full numerical simulations (with about 10^6 degrees of freedom). Moreover, an encouraging robustness of the reduced-order model has been observed, as it recovered the dynamics of the full system even for off-design conditions. Both accuracy and robustness are important prerequisites for a reduced-order model in control applications, and future efforts will focus on nonlinear model-predictive control applications based on our POD-DEIM models.

Acknowledgments

The authors acknowledge the stimulating and supportive environment at CTR during the 2014 Summer Program; in particular, we wish to thank the members of the aeroacoustic noise group for their encouraging feedback and many fruitful discussions.

REFERENCES

- ANTOULAS, A. C. 2004 *Approximation of Large-Scale Dynamical Systems, Advances in Design and Control*, vol. 6. SIAM Publishing.
- BARBAGALLO, A., SIPP, D. & SCHMID, P. J. 2009 Closed-loop control of an open cavity flow using reduced-order models. *J. Fluid Mech.* **641**, 1–50.
- CHATURANTABUT, S. & SORENSEN, D. C. 2010 Nonlinear model reduction via discrete empirical interpolation. *SIAM J. Sci. Comput.* **32**, 2737–2764.
- CHATURANTABUT, S. & SORENSEN, D. C. 2011 Application of POD and DEIM on dimension reduction of non-linear miscible viscous fingering in porous media. *Math. Comp. Model. Dyn.* **17**, 337–353.
- ITO, K. & RAVINDRAN, S. S. 1998 A reduced-order method for simulation and control of fluid flows. *J. Comput. Phys.* **143**, 403–425.
- LASSILA, T., MANZONI, A., QUARTERONI, A. & ROZZA, G. 2014 Model order reduction in fluid dynamics: challenges and perspectives. In *Reduced order methods for modeling and computational reduction*, pp. 235–273. Springer Verlag.
- FOSAS DE PANDO, M., SIPP, D. & SCHMID, P. J. 2012 Efficient evaluation of the direct and adjoint linearized dynamics from compressible flow solvers. *J. Comput. Phys.* **231**, 7739–7755.
- QUARTERONI, A. & ROZZA, G. 2014 *Reduced Order Methods for Modeling and Computational Reduction*. Springer Verlag.
- RAVINDRAN, S. S. 2002 Control of flow separation over a forward-facing step by model reduction. *Comput. Method. Appl. M.* **191**, 4599–4617.
- SAMIMY, M., DEBIASI, M., CARABALLO, E., SERRANI, A., YUAN, X., LITTLE, J. & MYATT, J. H. 2007 Feedback control of subsonic cavity flows using reduced-order models. *J. Fluid Mech.* **579**, 315–346.